Hindawi
Journal of Nanomaterials
Volume 2022, Article ID 1668206, 14 pages
https://doi.org/10.1155/2022/1668206

Research Article

Analytical and Numerical Analysis of the Squeezed Unsteady MHD Nanofluid Flow in the Presence of Thermal Radiation

Hakeem Ullah,[1] **Muhammad Arif Khan**,[1] **Mehreen Fiza**,[1] **Kashif Ullah**,[1] **Muhammad Ayaz**,[1] **and Seham M. Al-Mekhlafi**[2]

[1]*Department of Mathematics, Abdul Wali Khan University, Mardan, KP, Pakistan*
[2]*Department of Mathematics, Sanna University, Yemen*

Correspondence should be addressed to Seham M. Al-Mekhlafi; smdk100@gmail.com

Received 29 December 2021; Revised 9 March 2022; Accepted 14 March 2022; Published 31 March 2022

Academic Editor: Anwar Saeed

In this study, the unsteady squeezing nanofluid flow between two plates with thermal radiation has been investigated. The governing equations of the flow model have been transformed to a set of nonlinear ordinary differential equations (ODEs) from a set of partial differential equations (PDEs) using a suitable similarity variable. The optimal auxiliary function method (OAFM) and Runge–Kutta method of order 4 (RK method of order 4) are used for the solution of the modeled problem. The variation of the squeezing number, Prandtl number, Eckert number, and thermal radiation has been presented. The magnetic field resists the flow velocity, and the Prandtl number resists the temperature distribution. The increase in volume fraction decreases the velocity profile whereas increases the temperature profile. The skin friction coefficient and the Nusselt number are inversely proportional to S. The effect of increasing values of E_c is to decrease the skin friction coefficient C_f and the heat transfer rate Nu_x. The increasing value of φ increases the skin friction coefficient and decreases the heat transfer rate.

1. Introduction

The nanofluid consists of the nanometer particle size of the fluid having less than 10^-9nm, such as copper, aluminum, silver, silicon, aluminum oxides, and graphite. The base fluids are water, oil, and ethylene glycol. Choi et al. [1] introduced the term nanofluid and heat transfer features of the fluids, such as thermal conductivity is enriched by the addition of nanoparticles into it [2, 3]. The study of heat and mass transfer for squeezing unsteady viscous flow between two parallel plates has a wide range of physical applications, including lubrication systems, polymer processing, food processing, hydrodynamical machines, compression, and crop damage due to freezing, formation, and dispersion. Squeeze flow, also known as squeezing flow, squeezing film flow, or squeeze flow theory, is a flow in which a material is squeezed out between two parallel plates. Josef Stefan studied it in 1874 for the first time. There are several squeeze flow models that may be used to explain Newtonian and non-Newtonian fluids that are squeezed under various geometries and conditions. Squeeze flow is used in a variety of scientific and engineering areas, including welding engineering, and materials science, to name a few. Sheikholeslami et al. [4] used heat line analysis to simulate a two-phase simulation of nanofluid flow and heat transfer. Moreover, Sheikholeslami et al. [5] investigated the unsteady flow of a nanofluid squeezing between two parallel plates using the Adomian decomposition method (ADM). Also, the problem of squeezing flow between rotating disks has been studied by Hamza [6] and Bhattacharyya [7]. Magnetohydrodynamics (MHD) is the information of the magnetic assets of electrically conducting fluids. Plasmas, electrolytes, water, and liquid metals are examples of magneto fluids. Hannes Alfven [8] was the first who introduced the field of MHD. MHD has several applications in the field of industries and engineering such as plasma, crystal growth, MHD sensors, liquid-metal cooling of MHD casting, MHD power generation, and magnetic drug targeting. MHD depends on the strength of the magnetic field; the stronger the magnetic field, the greater is MHD effects and vice versa. MHD includes plasmas, molten

metals, saltwater, and electrolytes. [9–13]. Seddiqui, Domairy, and Aziz et al. [14, 15] explored two-dimensional MHD squeezing flow between parallel plates and parallel disc. Magnetic nanofluid is a one-of-a-kind material that combines the qualities of a liquid with a magnetic material [16]. Magneto-optical wavelength filters [17, 18], optical modulators, [19], nonlinear optical materials [20], tunable optical fiber filters [21], optical gratings, and optical switches have all been discovered to use such fluids [22]. Changing the magnetic field can change a lot of the physical features of these fluids. They also served as an excellent model system for fundamental investigations. Manipulation of nanoparticles with carbon nanotubes has recently been shown to result in increased thermal conductivity. The thermal characteristics of nanofluids are the parameters that are critical to the performance of nanofluids. Thermal conductivity, specific heat, viscosity, and heat transfer coefficient are the four variables. Solar collector thermal performance is mostly determined by how thermal characteristics behave under various operating situations. Temperature, environmental conditions, type of base fluid, particle size and form of the nanoparticle, and volume concentration are all operating parameters. Taking into account all of these factors, choosing the right nanofluid is critical for optimum performance. Based on this idea, scientist studies many important flow models for various physical aspects [23–26]. Explicit Runge–Kutta techniques have become popular for wave simulations due to their great accuracy and low memory requirements [27]. The traditional fourth-order Runge–Kutta technique requires three memory places per dependent variable [28]; however, low-storage approaches may be constructed that only require two memory sites per dependent variable [29]. A third-order Runge–Kutta technique can readily accomplish this characteristic, while a fourth-order approach requires an additional stage [30]. Because the evaluation of the derivative function is the fundamental cost of integration, and each level necessitates a function evaluation, the new stage implies a large rise in cost. Some of the recent development in the related field can be seen in [26, 31–42]. In this paper, we propose the OAFM [43, 44] for the squeezed unsteady MHD nanofluid flow in the presence of thermal radiation. The validity of OAFM is based on the auxiliary function which optimally controls the convergence of the solution. The efficiency of OAFM is proved in comparison to the numerical solutions obtained by Runge–Kutta method of order 4. In the present work, we show how solutions to the modeled problem can be obtained using OAFM, without the need for complex and complicated calculations with low specification of computer with high accuracy. Moreover, OAFM presented here is less computational work and simple in applications at the first iteration. Up to now, the squeezed unsteady MHD nanofluid flow in the presence of thermal radiation has not been studied. The purpose of this study is to provide an analytical solution of the squeezed unsteady MHD nanofluid flow in the presence of thermal radiation by using the newly developed method OAFM. In the above-mentioned problem, analytical and numerical methods are used for the solution of the problem. The numerical methods required the linearization and discretization techniques and huge computer memory with operating time; we show how solutions to the boundary value problem can be obtained using OAFM, without the need for complex and involved mathematical algorithms, and at a relatively low computing memory and easy approach with high accuracy at the first iteration.

2. Basic Mathematical Theory of OAFM [43, 44]

Let us look at the OAFM for the differential equation

$$L(f(\eta)) + s(\eta) + N(f(\eta)) = 0, \tag{1}$$

where L, N denotes the linear and nonlinear operators; s denotes the source function, $f(\kappa)$, and is an unknown function at this stage; the initial/boundary conditions are

$$B\left(f(\eta), \frac{df(\eta)}{d\eta}\right) = 0. \tag{2}$$

Because finding an accurate solution to severely nonlinear equations is extremely difficult, the proposed approximation is as follows:

$$f(\eta, E_k) = f_u(\eta) + f_1(\eta, E_c), k = 1, 2, \cdots s. \tag{3}$$

Using Equation (3) in Equation (1), we have

$$L(f_0(\eta)) + L(f_1(\eta, E_k)) + s(\eta) + N(f_0(\eta) + f_1(\eta, E_k)) = 0, \tag{4}$$

where $E_k, k = 1, 2 \cdots s$ are control convergence parameters to be determined.

The initial approximation is determined as

$$L(f_0(\eta)) + s(\eta) = 0, \quad B\left(f_0(\eta), \frac{f_0(\eta)}{d\eta}\right) = 0. \tag{5}$$

The first approximation is obtained as

$$L(f_1(\eta, E_k)) + N(f_0(\eta) + f_1(\eta, E_k)) = 0, B\left(f_1(\eta).\frac{f_1(\eta)}{d\eta}\right) = 0. \tag{6}$$

The nonlinear term is expressed as

$$D_1, D_2 N(f_o(\eta) + f_1(\eta, E_k)) = N(f_o(\eta)) + \sum_{i=1}^{\infty} u(t, E_k) N(f_o(\eta)). \tag{7}$$

The last term in Equation (7) seems difficult to solve, so to avoid this difficulty and to fast the convergence of the

solution. Equation (6) can be written as

$$L(f_1(\eta, E_k)) + D_1((f_0(\eta), E_m)F(N(f_0(\eta)))) + D_2(f_0(\eta), E_n) = 0,$$

$$B\left(f_1(\eta, E_k)\frac{df_1(\eta), E_k)}{d\eta}\right) = 0, n = 1, 2 \cdots q, m = q + 1, q + 2, \cdots s, \tag{8}$$

where D_1, D_2 are optimal auxiliary which depends on $f_0(\kappa)$ and E_n, E_m and $F(N(f_0(\kappa)))$ is a function which depends on the expression appearing within the nonlinear term of $N(f_0(\kappa))$. The optimal auxiliary function should be expressed in the sum form of $f_o(\kappa)$ such as if $f_o(\kappa)$ are polynomial. Exponential and trigonometric then D_1, D_2 would be the sum of polynomial, exponential, and trigonometric, respectively. Also $f_o(\kappa)$ would be the exact solution of the original problem, if $N(f_o(\kappa)) = 0$. The optimal auxiliary functions can be obtained from method of least square, collocation method Galerkan Ritz methods.

2.1. Convergence of the Method. In order to obtain the convergent solution, we calculate the optimal constants also known as control convergence constant by method of least squares: These optimal constants are resubmitted into original equation to get the series solution.

$$J(E_1, E_2, \cdots E) = \int_1 R^2(\eta, E_1, E_2, \cdots E_s)d\eta, \tag{9}$$

where I is equation domain.

The unknown constants are established as

$$\frac{\partial J}{\partial E_1} = \frac{\partial J}{\partial E_2} = \cdots \frac{\partial J}{\partial E_n} = 0. \tag{10}$$

The mth order approximate solution can be obtained by these constants so obtained.

3. Formulation of the Problem

The flow and heat transfer of two-dimensional unsteady squeezing nanofluid via the lateral plates is observed in this study, as shown in Figure 1.

At any nondimensional time t, the distance between the two plates is given as

$$z = \pm l(1 - at)^{\frac{1}{2}} = \pm h(t), \text{for } a > 0. \tag{11}$$

The two plates are squeezed until they touch each other at $1/\alpha$, whereas at $\alpha < 0$, the two plates are separated. Here, α is a constant, l is the initial position (at $t = 0$), and z is the axial coordinate, which is obviously zero from the flow zone, with the flow model evaluated along the x and y axes. The nondimensional time throughout the flow is represented by the variable t. The heat source and viscous dissipation effect as a result of friction caused by fluid flow shear are both protected. As a result, this behavior occurs when the Eckert number is very high. Meanwhile, the copper material was enclosed in a nanofluid. A uniform magnet is used perpendicular to the flow. The following are the governing equations:

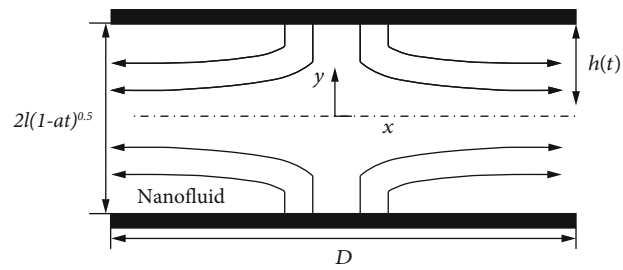

Figure 1: Geometry of the flow problem.

$$\frac{\partial u}{\partial x} + \frac{\partial v}{\partial y} = 0, \tag{12}$$

$$\frac{\partial u}{\partial x} + u\frac{\partial v}{\partial y} + v\frac{\partial u}{\partial y} = -\frac{1}{\rho_{nf}}\frac{\partial p}{\partial y} + \frac{\mu_{nf}}{\rho_{nf}}\left(\frac{\partial^2 v}{\partial x^2} + \frac{\partial^2 u}{\partial y^2}\right) - \frac{\sigma {B_0}^2}{\rho_{nf}}u, \tag{13}$$

$$\frac{\partial v}{\partial t} + u\frac{\partial v}{\partial x} + v\frac{\partial v}{\partial y} = -\frac{1}{\rho_{nf}}\frac{\partial p}{\partial y} + \frac{\mu_{nf}}{\rho_{nf}}\left(\frac{\partial^2 v}{\partial x^2} + \frac{\partial^2 v}{\partial y^2}\right), \tag{14}$$

$$\frac{\partial T}{\partial t} + u\frac{\partial T}{\partial x} + v\frac{\partial T}{\partial y} = \frac{knf}{(\rho Cp)_{nf}}\left(\frac{\partial^2 T}{\partial x^2} + \frac{\partial^2 T}{\partial y^2}\right) + \frac{\mu_{nf}}{(\rho Cp)_{nf}}\left(4\left(\frac{\partial u}{\partial y}\right)^2\right) - \frac{1}{\rho Cp}\frac{\partial qr}{\partial y}. \tag{15}$$

The velocities in the x and y directions are represented by u and v, respectively. While p, T, $T\infty$, f, and k_{nf} are the effective density, dynamic viscosity, heat capacity, and thermal conductivity of the nanofluid; ρnf, μnf, (ρCp), and k_{nf} are the effective density, dynamic viscosity, heat capacity, and thermal conductivity of the nanofluid, respectively.

$$\rho_{nf} = (1 - \phi)\rho_f + \phi\rho_{p'}, \tag{16}$$

$$\left(\rho C_p\right)_{nf} = (1 - \phi)\left(\rho C_p\right)_f + \phi\left(\rho C_p\right)_{p'}, \tag{17}$$

$$\mu_{nf} = \frac{\mu_f}{(1 - \phi)^{2.5'}} \text{ (Brinkman)}, \tag{18}$$

$$\frac{k_{nf}}{k_f} = \frac{k_s + 2k_f - 2\phi\left(k_f - k_s\right)}{k_s + 2k_f + 2\phi\left(k_f - k_s\right)} \text{ (Maxwell-Garnett)}. \tag{19}$$

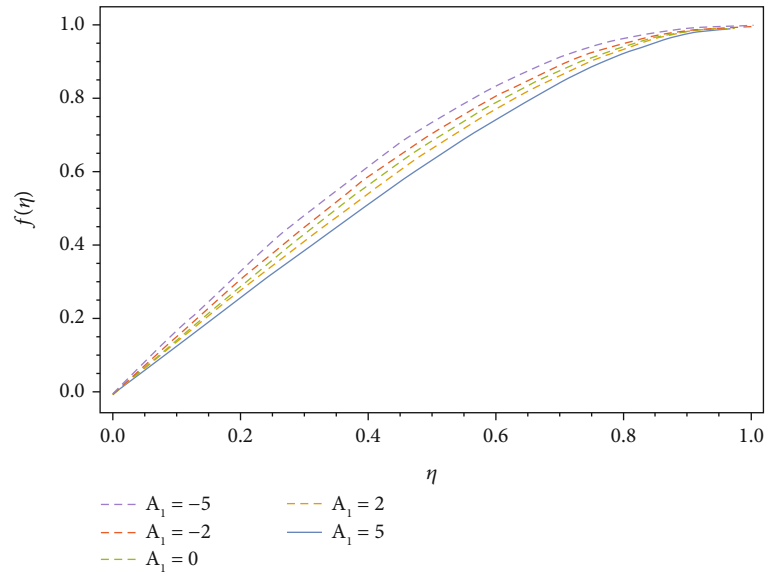

Figure 2: Effect of the A_1 on the f.

Subject to the following boundary conditions

$$v = v_w = \frac{dh}{dt'} T = T_H \text{ at } y = h(t), v = \frac{\partial u}{\partial y} = \frac{\partial T}{\partial y} = 0 \text{ at } y = 0. \tag{20}$$

The radiative heat flux in Equation (4) is given by the Rosseland formula as

$$q_r = -\frac{4\sigma^*}{3k^*}\frac{\partial T^4}{\partial y}. \tag{21}$$

The Stefan-Boltzmann constant and the mean absorption number, respectively, are $\sigma *$ and $k *$. We assume that the temperature variation among the flow is greatly constrained, and that the expression T^4 may be regarded a linear function of temperature, based on various research, As a result, T^4 is enlarged by disregarding the higher-order terms and utilizing Taylor series expansion about T.

$$T^4 4T_\infty{}^3 - 3T_\infty^4. \tag{22}$$

Substituting Equations (21) and (22) into Equation (15), we obtain

$$\frac{\partial T}{\partial t} + u\frac{\partial T}{\partial x} + v\frac{\partial T}{\partial y} = \frac{k_{nf}}{(\rho C_p)_{nf}}\left(\frac{\partial^2 T}{\partial x^2} + \frac{\partial^2 T}{\partial y^2}\right) + \frac{\mu_{nf}}{(\rho C_p)_{nf}}\left(4\left(\frac{\partial u}{\partial x}\right)^2\right) + \frac{32\sigma^* T_\infty^3 \partial^2 T}{3\rho C_p k^* \partial y^2}. \tag{23}$$

To begin, introduce the following quantities:

$$\eta = \frac{y}{\left[l(1-\alpha t)^{1/2}\right]}, u = \frac{ax}{[2(1-\alpha t)]} f'(\eta), v = -\frac{al}{[2(1-\alpha t)]} f(\eta), \theta = \frac{T}{T_H}, A_1 = (1-\phi) + \phi\frac{\rho_s}{\rho_f}, N = \frac{4\sigma^* T_\infty^3}{k_{f\rho} C_p k^*}, \tag{24}$$

$$f^{iv} - SA_1(1-\phi)^{2.5}\left(\eta f''' + 3f'' + f'f'' - ff'''\right) - M^2 f' = 0, \tag{25}$$

$$(12A_3 + 16A_2 N)\theta'' + 3\,\mathrm{Pr}\, SA_2\left(f\theta' - \eta\theta'\right) + \frac{3\,\mathrm{Pr}\, E_c}{(1-\phi)^{2.5}}\left(f''^2 + 4\delta^2 f'^2\right) = 0. \tag{26}$$

where N denotes heat/thermal radiation as defined by Equation (10), and A_2 and A_3 denote dimensionless constants as defined by

$$A_2 = (1-\phi) + \phi\frac{(\rho C_p)_s}{(\rho C_p)_f}, A_3 = \frac{k_{nf}}{k_f}. \tag{27}$$

Equations (25) and (26) must now bssssse solved in the context of

$$f(0) = 0, f(1) = 1, f'(1) = 0, \theta'(0) = 0, \theta(1) = 1. \tag{28}$$

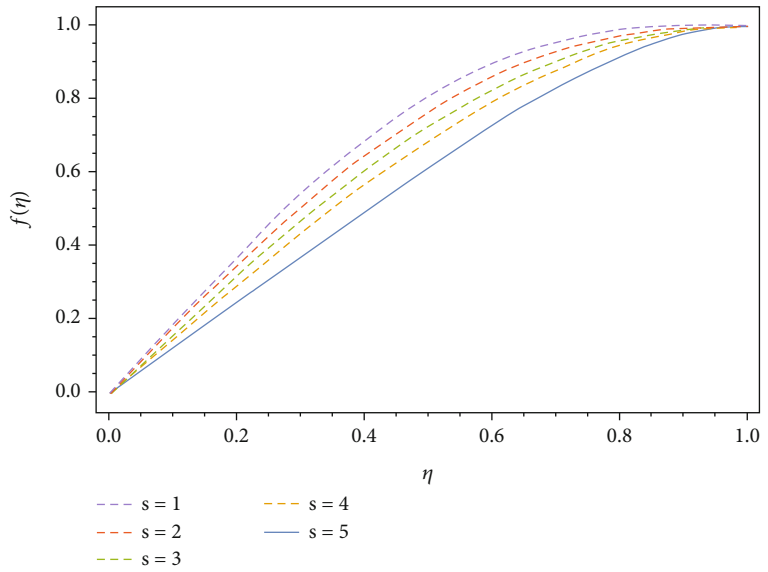

Figure 3: Effect of s on f.

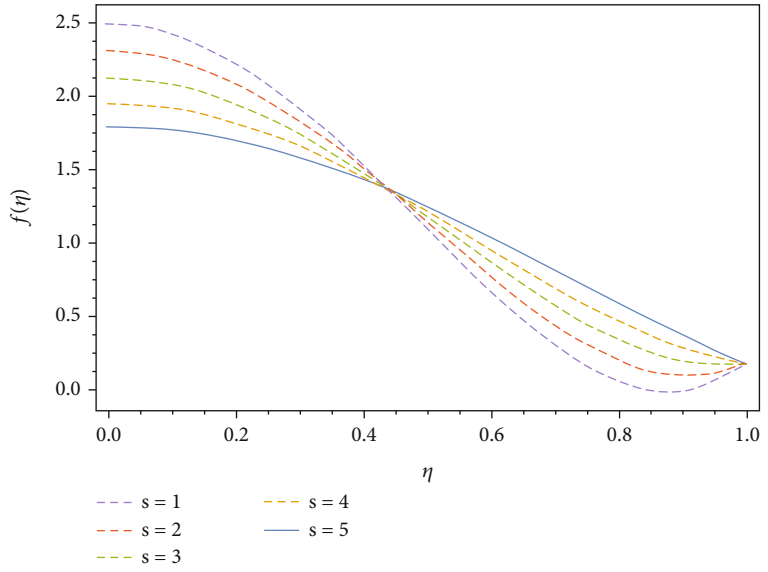

Figure 4: Effect of S on f'.

Here, S is the squeezing integer; P_r and Ec are the Prandtl and Eckert numbers, respectively.

$$S = \frac{al}{2\nu_f}, P_r = \frac{\mu_f (\rho C_p)_f}{\rho_f k_f}, E_c = \frac{\rho_f}{(\rho C_p)_f}\left(\frac{ax}{2(1-\alpha t)}\right)^2, \\ \delta = \frac{1}{x}.M^2 = \frac{\sigma {B_0}^2}{\rho_{nf}}\left(\frac{ax}{2(1-\alpha t)}\right), f''(0) = 0, \tag{29}$$

The following quantities are categorically used for practical interest as defined

$$C_f = \frac{\mu_{nf}(\partial u/\partial y)_{y=h(t)}}{\rho_n f^{v_w^2}}, N_u = \frac{-lk_{nf}(\partial T/\partial y)_{y=h(t)}}{kT_H}. \tag{30}$$

Equation (24) provides the following result:

$$C_f = \frac{l^2}{x^2(1-\alpha t)\ \mathrm{Re}_x C_f} = A_1(1-\phi)^{2.5} f''(1), \\ Nu^* = \sqrt{1-\alpha t} Nu = -A_3\theta'(1). \tag{31}$$

The linear and nonlinear operators of Equations (11) and (12) are

$$L(f(\kappa)) = f^{iv}(\kappa) \tag{32}$$

$$L(\theta(\kappa)) = \theta''(\kappa) \tag{33}$$

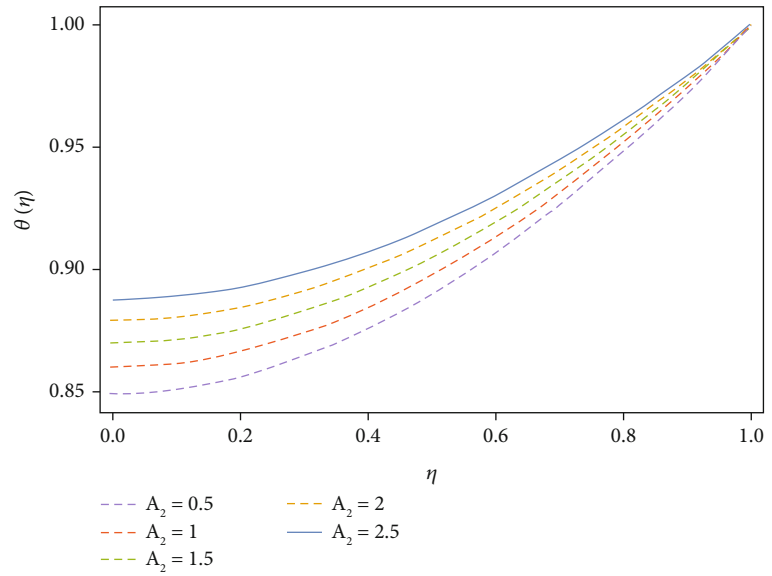

Figure 5: Effect of A_2 on Θ.

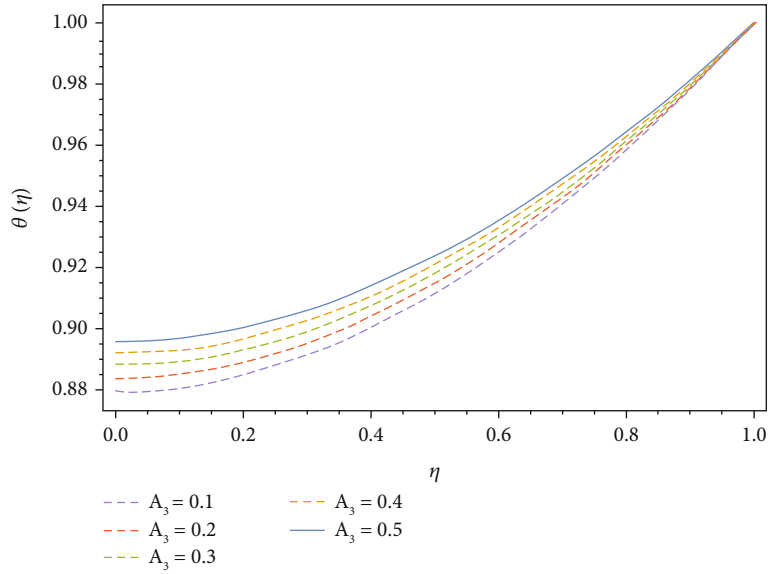

Figure 6: Effect of A_3 on Θ.

$$N(f(\kappa)) = -SA(1-\phi)^{2.5}\left(\eta f''' + 3f'' + f'f'' - ff'''\right) - M^2 f' \tag{34}$$

$$N(\theta(\kappa)) = 3\ \mathrm{Pr}\ SA_2\left(f\theta' - \eta\theta'\right) + \frac{3\ \mathrm{Pr}\ Ec}{(1-\phi)^{2.5}}\left(f''^2 + 4\delta^2 f'^2\right) \tag{35}$$

From Equation (5), we have

$$f^{iv}(\kappa) = 0\ f(0) = 0, f''(0) = 0, f(1) = 1, f'(1) = 0,$$
$$\theta''(\kappa) = 0\ \theta'(0) = 0, \theta(1) = 1, \tag{36}$$

has solution as

$$f_0(\kappa) = \frac{1}{2}\left(3\kappa - \kappa^3\right),$$
$$\theta_0(\kappa) = 1. \tag{37}$$

Based on Equation (23), we get

$$N(f_o(\kappa)) = -SA_1(1-\phi)^{2.5}\left(18\kappa^2 - 18\kappa - 6\eta\right),$$
$$N(\theta_o(\kappa)) = \frac{3\ \mathrm{Pr}\ E_c}{(1-\phi)^{2.5}}\left(36\delta\kappa^4 + 36\kappa^2 + 9\delta\right). \tag{38}$$

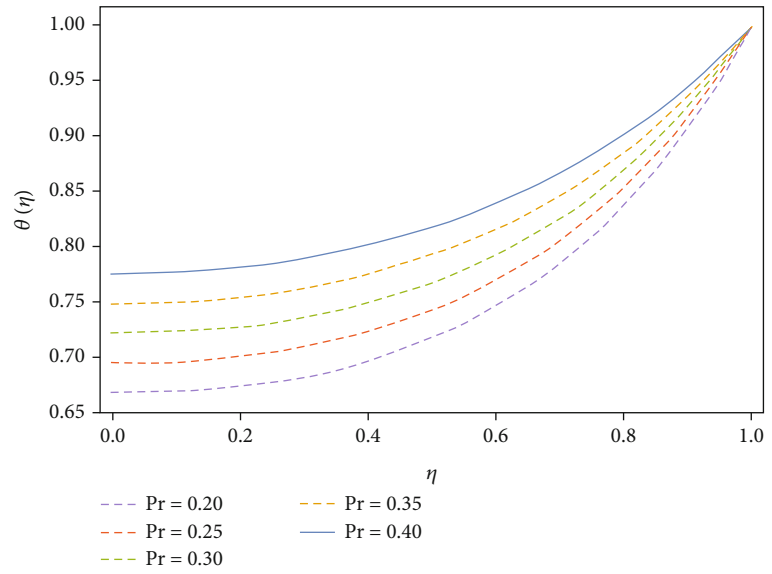

Figure 7: Effect of Pr on Θ.

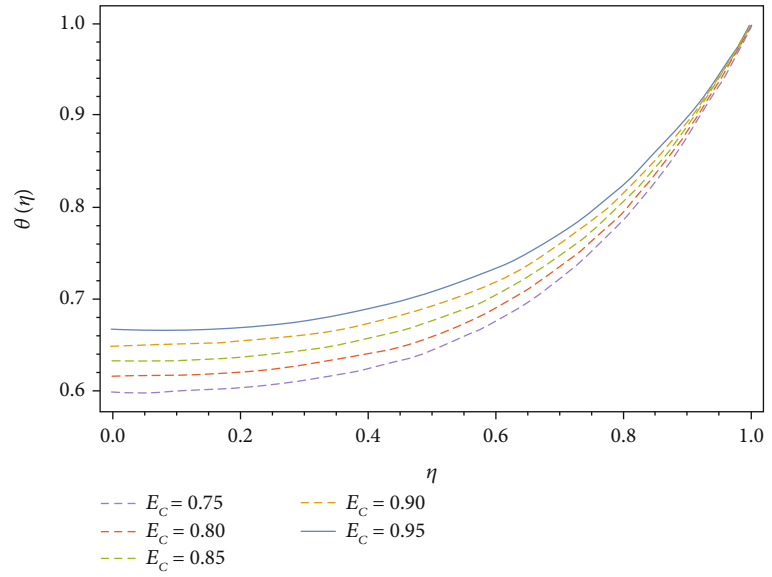

Figure 8: Effect of E_c on Θ.

In the first approximation based on Equations (8), (32), (33), and (24), we get

$$f^{iv}(\kappa) + D_1\left(\kappa, \kappa^2, \kappa^3, E_m\right)\left(-SA_1(1-\phi)^{2.5}\left(18\kappa^2 - 18\kappa - 6\eta\right)\right) + D_2\left(\kappa, \kappa^2, \kappa^3, E_n\right) = 0,$$

$$\theta''(\kappa) + D_3\left(\kappa, \kappa^2, \kappa^3, E_p\right)\left(\frac{3\ \mathrm{Pr}\ E_c}{(1-\phi)^{2.5}}\left(36\delta\kappa^4 + 36\kappa^2 + 9\delta\right)\right) + D_4\left(\kappa, \kappa^2, \kappa^3, E_r\right) = 0. \tag{39}$$

with boundary conditions

$$f(0) = 0, f''(0) = 0, f(1) = 1, f'(1) = 0, \quad \theta'(0) = 0, \theta(1) = 1. \tag{40}$$

The OAF can be chosen freely as

$$D_1(f_o(\kappa), E_m) = -(E_1 + E_2\kappa),$$

$$D_2(f_o(\kappa), E_n) = -(E_1 + E_2\kappa)\kappa - \left(E_5 + E_6\kappa + E_7\kappa^2\right)\kappa^2,$$

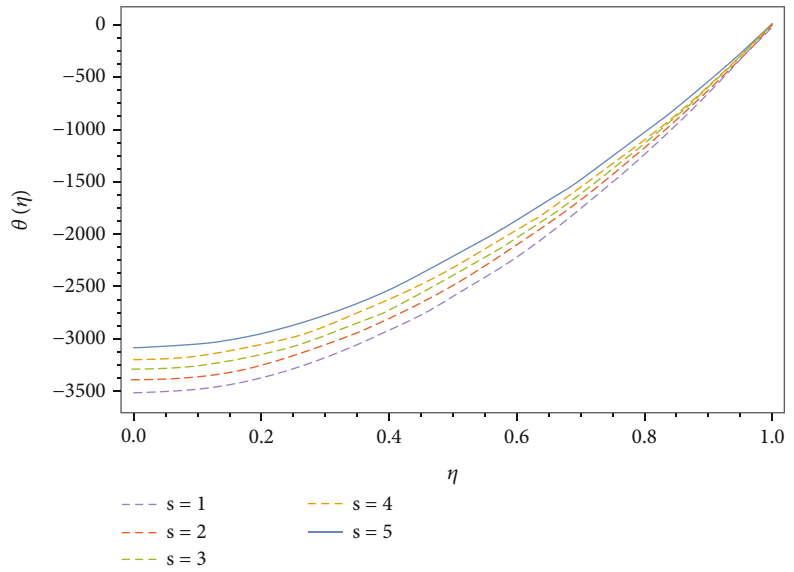

Figure 9: Effect of s on Θ.

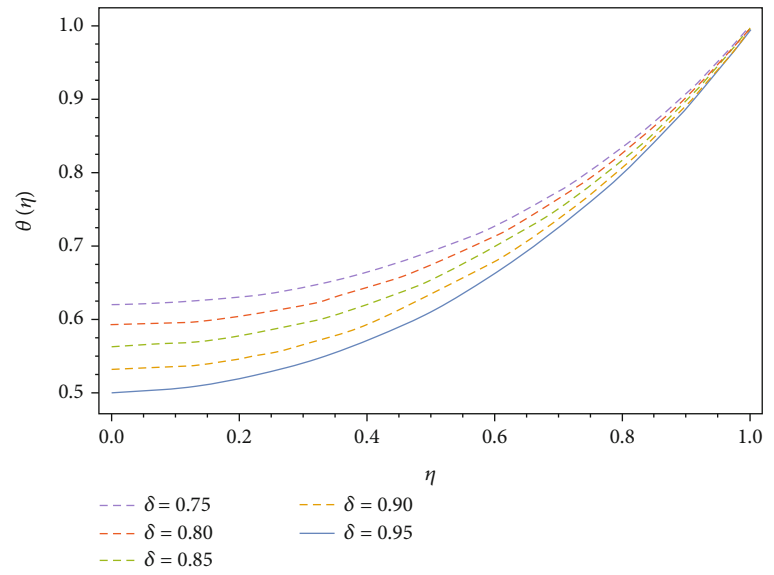

Figure 10: Effect of δ on Θ.

$$D_3\left(f_o(\kappa), E_p\right) = 0,$$

$$D_4(f_o(\kappa), E_r) = -(E_8 + E_9\kappa)\kappa - \left(E_{10} + E_{11}\kappa + E_{12}\kappa^2\right)\kappa^2. \tag{41}$$

We obtained the first approximate solution

$$f^{iv}(\kappa) + D_1\left(\kappa, \kappa^2, \kappa^3, E_m\right)\left(-SA_1(1-\phi)^{2.5}\left(18\kappa^2 - 18\kappa - 6\eta\right)\right) + D_2\left(\kappa, \kappa^2, \kappa^3, E_n\right) = 0,$$

$$\theta''(\kappa) + D_3\left(\kappa, \kappa^2, \kappa^3, E_p\right)\left(\frac{3\ \mathrm{Pr}\ E_c}{(1-\phi)^{2.5}}\left(36\delta\kappa^4 + 36\kappa^2 + 9\delta\right)\right) + D_4\left(\kappa, \kappa^2, \kappa^3, E_r\right) = 0. \tag{42}$$

And its solution is given as by putting the values of the optimal constants obtained from the method of least square.

$$f(\kappa) = -\frac{1}{280}\kappa\left(140\left(-3 + \kappa^2\right) + chst\left(-26 + \kappa^2\right)\left(-1 + \kappa^2\right)^2\right),$$

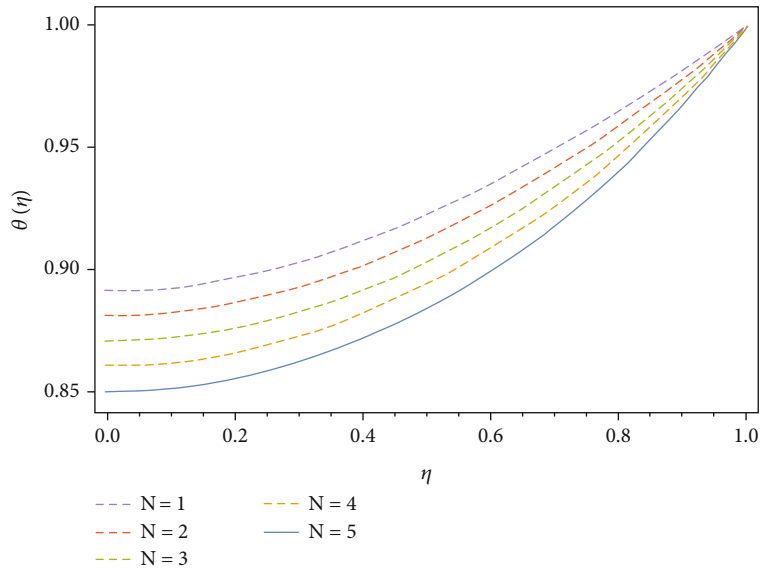

Figure 11: Effect of N on Θ.

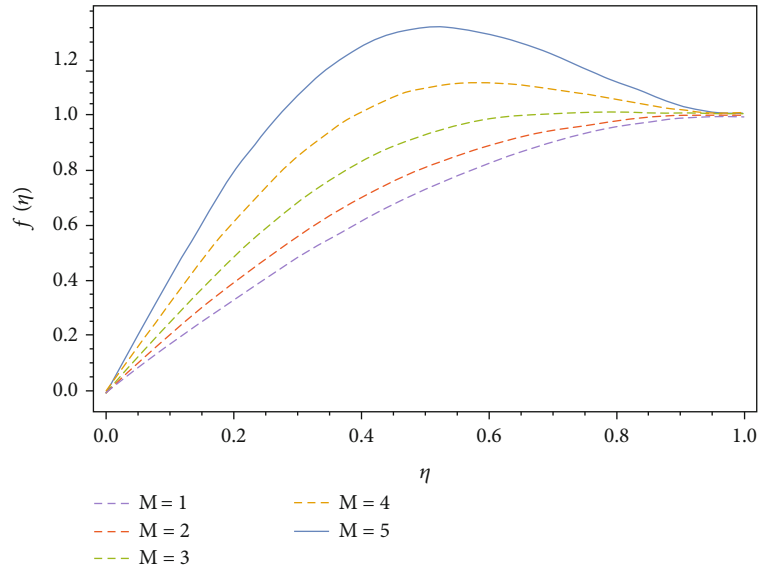

Figure 12: Effect of M on $f(\eta)$.

$$\theta(\kappa) = \frac{20t + 3h\left(-1+\kappa^2\right)\left(15\ \mathrm{Pr}\ Q\left(1+\kappa^2\right) + 2t\left(11 - 4\kappa^2 + \kappa^4\right)\delta^2\right)}{20t}. \tag{43}$$

4. Numerical Method of Solution

The differential Equations (25) and (26) along with the side condition (28) have been solved using the fourth-order Runge–Kutta method (FORKM) along with the shooting technique. The nonlinear Equations (25) and (26) of fourth and second order are reduced to a set of six first-order simultaneous equations as follows:

$$f_1 = f, f_2 = f', f_3 = f'', f_4 = f''', f_5 = \theta, f_6 = \theta', f_4' = f'''', f_6' = \theta'', \tag{44}$$

$$f_4' = SA_1(1-\phi)^{2.5}\left(\eta f_4 + 3f_3 + f_2 f_3 - f_1 f_4\right) - M^2 f', \tag{45}$$

$$f_6' = -3\ \mathrm{Pr}\ SA_2(f_1 f_6 - \eta f_6) - \frac{3\ \mathrm{Pr}\ Ec}{(1-\phi)^{2.5}} \frac{\left(f_3'' + 4\delta^2 f_2''\right)}{12A_3 + 16A_2 N}. \tag{46}$$

The boundary condition now became

$$f_1(0) = 0, f_3(0) = 0, f(1) = 0, f_2(1) = 0, f_4(1) = 1, f_3(0) = 0. \tag{47}$$

Solving of this system, six initial conditions are needed, while only three conditions are available. Some initial conditions are not given in the problem. Here, the values of f, f'

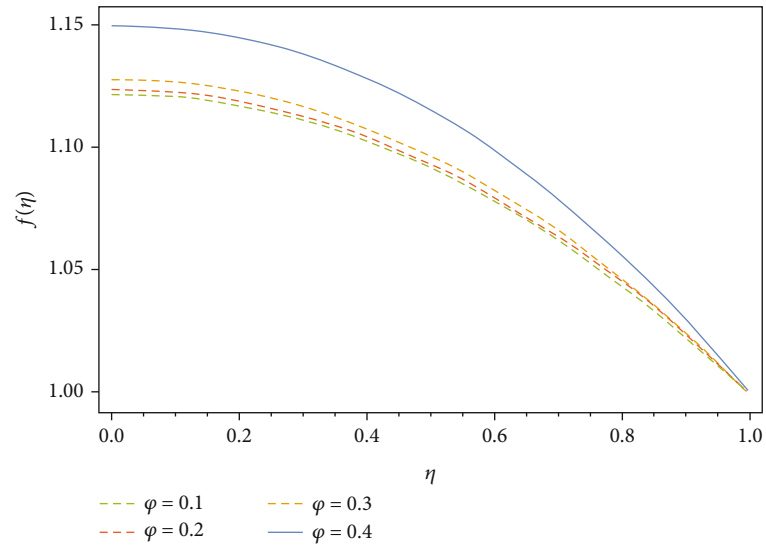

Figure 13: Effect of volume friction ϕ on $f(\eta)$.ss

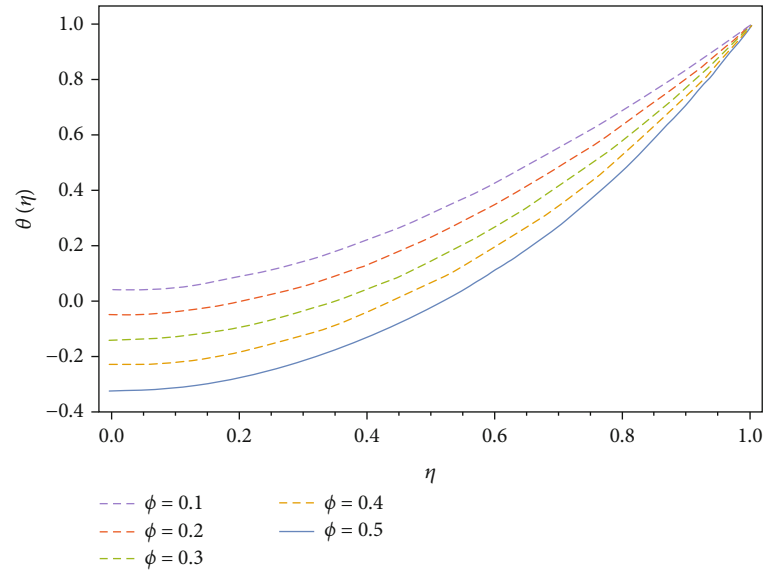

Figure 14: Effect of volume friction ϕ on $\theta(\eta)$.

and f''' are known as $\eta \longrightarrow 1$. These three-end conditions are used to produce the three unknown initial conditions by applying the shooting technique.

5. Results and Discussion

5.1. Graphical Discussion. The main focus of the study is to develop a mathematical model of an unstable nanofluid flow squeezed between parallel plates, as illustrated in Figure 1. Figure 2 shows the effect of A_1 on the velocity profile f. An increase in A_1 causes to increase the velocity profile f. Figures 3 and 4 demonstrate the influence of the squeeze number on the velocity profile. The motion of the plates represented by squeezing flow is indicated by the squeeze number S. When $S > 0$, the plates are moving separately, but when $S < 0$, the plates are moving collectively. Positive and negative squeezing values have distinct effects on the velocity profile. The velocity rises when the absolute value of the squeeze number is 0.5, but drops when it is >0.5. An increase in the stretching parameter causes to increase the velocity profile. The strecthing parameter assists the flow velocity. Figure 5 shows the effect of A_2 on the temperature profile $\theta(\eta)$. The temperature profile increases by increasing A_2. Also, the effect of A_3 on the temperature profile $\theta(\eta)$ is given in Figure 6. By increasing the values of A_3, a reverse effect as compared to A_2 has been observed. The influence of the Prandtl number P_r on temperature distributions is seen in Figure 7. With a large number of P_r, the temperature distribution obviously decreases, whereas with a small number of P_r, it grows. Fluids with a low Prandtl number have a higher thermal diffusivity than fluids with a high Prandtl number. A high P_r causes the thermal boundary layer to

Table 1: Comparison of the value of rate of velocity profile $f(\eta)$ for different value of η when $S = 0.90$, Pr = 0.3, $Ec = 0.5$, $A_1 = 0.1$, $A_2 = 0.5$, $A_3 = 0.7$, $\delta = 0.6$, $M = 1$.

	OAFM	4th RKM	Absolute error
0	0.	0.	0.00000000
0.1	0.119482	0.119482	1.245789×10^{-17}
0.2	0.241044	0.241044	1.02145×10^{-17}
0.3	0.365079	0.365079	3.21458×10^{-17}
0.4	0.490248	0.490248	2.01245×10^{-17}
0.5	0.613586	0.613586	1.02158×10^{-17}
0.6	0.730601	0.730601	3.12458×10^{-17}
0.7	0.835395	0.835395	2.32489×10^{-17}
0.8	0.920813	0.920813	2.87963×10^{-17}
0.9	0.97866	0.97866	1.98756×10^{-17}
1	1.	1.	1.05896×10^{-16}

decrease as a result. The impact is much more noticeable for a small number of P_r because the thermal boundary layer thickness is so high. The impact of Eckert number and Prandtl number on the temperature profile is shown in Figure 8. It is observed that the temperature rises substantially with rising E_c. The effect of s and δ on the temperature profile is given in Figures 9 and 10. Again, an increase in s and δcauses to decrease the temperature profile. The effect of the thermal radiation N on the temperature profile is given in Figure 11. The increase in thermal radiations causes to increase the temperature profile, since the thermal radiations increase the kinetic energy of the particles and their collision is caused to rise the temperature profile. The effect of magnetic field on the velocity profile is presented in Figure 12. The increase in magnetic field M reduces the velocity profile, since the magnetic field is applied perpendicular to the flow, and hence the conducting fluid particles feel the opposite force of magnetic field and hence reduce the velocity profile. The effect of volume fraction of nanofluid on the velocity and temperature profiles is given in Figures 13 and 14, respectively. The increase in volume fraction ϕ decreases the velocity profile whereas increases the temperature profile.

5.2. Tables' Discussion. The results of OAFM are validated in comparison with the results obtained from the Runge–Kutta method of order 4 along with absolute errors as given in Tables 1 and 2. The OAFM results obtained at just one iteration provide us a simple way to control the convergence and nearly identical to the results obtained from RKM fourth-order method. The effects of the squeeze number S on the skin friction coefficient, Cf, and the Nusselt number, Nu_x, are given in Table 3. From Table 3, it is obvious that the skin friction coefficient and the Nusselt number are inversely proportional to S. Table 4 displays the effects of the skin friction coefficient and the Nusselt number for different values of the Eckret number. It is noticed from the table that the effect of increasing values of Ec is to decrease the skin friction coefficient, Cf, and the heat transfer rate Nu_x. Further, from Table 5, it is concluded that the increasing value of M decreases the skin friction coefficient and increases the heat rate. The effects of the nanoparticle volume fraction φ on the skin friction coefficient Cf Nusselt number (the

Table 2: Comparison of the value of rate of velocity profile $\phi(\eta)$ for different value of η when $S = 0.90$, Pr = 0.3, $Ec = 0.5$, $A_1 = 0.1$, $A_2 = 0.5$, $A_3 = 0.7$, $\delta = 0.6$, $M = 1$.

η	OAFM	4th RKM	Absolute error
0	0	0	0
0.1	0.14866782146738375	0.14866782146738370	5.3241×10^{-17}
0.2	0.29447924328271025	0.29447924328271020	5.3243×10^{-17}
0.3	0.4345297029288129	0.4345297029288122	5.3246×10^{-17}
0.4	0.5658641096465703	0.5658641096465697	5.3247×10^{-17}
0.5	0.6854800169389675	0.6854800169389669	5.3249×10^{-17}
0.6	0.7903318397285185	0.7903318397285178	5.3253×10^{-17}
0.7	0.8773361110067814	0.8773361110067808	5.3256×10^{-17}
0.8	0.9433777722643691	0.9433777722643686	5.3259×10^{-17}
0.9	0.9853174912829916	0.9853174912829909	5.3262×10^{-17}
1	1.0000000000000002	1.00000000000000007	1.3263×10^{-16}

Table 3: Comparison of skin friction and Nusselt numbers for various values of s.

s	C_f	Nu_x
1	-1.24578	0.145875
2	-2.65862	0.0254863
3	-3.54879	0.0354856
4	-3.998547	0.0421586
5	-4.214585	0.0015482

Table 4: Comparison of skin friction and Nusselt numbers for various values of E_c.

Ec	C_f	Nu_x
1	-1.56896	0.025486
2	-2.48523	0.052463
3	-2.012458	0.078563
4	-2.000458	0.0965482

Table 5: Comparison of skin friction and Nusselt numbers for various values of M.

M	C_f	Nu_x
1	-1.53624	0.0215463
2	-1.68459	0.0020012
3	-1.89654	0.015362
4	-2.12546	0.012156

Table 6: Comparison of skin friction and Nusselt numbers for various values of φ.

φ	C_f	Nu_x
0.10	-1.214655	0.045236
0.20	-1.284562	0.041256
0.30	-1.2954632	0.031256
0.40	-2.59632	0.021548

heat transfer rate) Nu are given in Table 6. From this table, it is concluded that the increasing value of φ increases the skin friction coefficient and decreases the heat transfer rate.

6. Conclusions

In this study, a new analytical method is suggested for the solution of the model problem. We obtain the first-order series solution for the governing equations of the model problem and achieved the first-order solution with high accuracy. For the accuracy and validity of OAFM, results are compared with numerical method. For comparison, it is concluded that the OAFM is very accurate and simple in application. OAFM is very easy in applicable to high nonlinear initial and boundary value problems even if the nonlinear initial/boundary value problem does not contain the small parameter. In comparison with other analytical methods, OAFM is very easy in applicability and provides us good results of more complex nonlinear initial/boundary value problems. OAFM contains the optimal auxiliary constants through which we can control the convergence as OAFM contains the auxiliary functions D_1, D_2, D_3, E_4 in which the optimal constants E_m, E_n, E_r, E_p and the control convergence parameters exist to play an important role to get the convergent solution which is obtained rigorously. The computational work in OAFM is less when compared to other methods, and even a low specification computer can do the computational work easily. The less computational work and rapid convergent solution at just the first iteration enable us to implement this efficient method in our future work for more complex models arising from real-world problems. The numerical method required maximum space and time as compared to OAFM is the short method and is very rapidly convergent. Numerical methods required to have large computational work and required the latest computer for computational work.

Based on the results and discussion, some points are presented here:

(i) The motion of the plates represented by squeezing flow is indicated by the squeeze number S. When $S > 0$, the plates are moving separately, but when $S < 0$, the plates are moving collectively. Positive and negative squeezing values have distinct effects on the velocity profile. The velocity rises when the absolute value of the squeeze number is 0.5, but drops when it is >0.5

(ii) With a large number of P_r, the temperature distribution obviously decreases, whereas with a small number of P_r, it grows. Fluids with a low Prandtl number have a higher thermal diffusivity than fluids with a high Prandtl number. A high P_r causes the thermal boundary layer to decrease as a result. The impact is much more noticeable for a small number of P_r because the thermal boundary layer thickness is so high

(iii) The increase in magnetic field M reduces the velocity profile, since the magnetic field is applied perpendicular to the flow, and hence, the conducting fluid particles feel the opposite force of magnetic field and hence reduce the velocity profile

(iv) The increase in volume fraction ϕ decreases the velocity profile whereas increases the temperature profile

(v) An increase in s and δcauses to decrease the temperature profile

(vi) The skin friction coefficient and the Nusselt number are inversely proportional to S

(vii) The effect of increasing values of E_c is to decrease the skin friction coefficient, Cf, and the heat transfer rate, ssNu$_x$

(viii) The increasing value of φ increases the skin friction coefficient and decreases the heat transfer rate

Abbreviations

a, b, c: Constants
$\widetilde{B}$: Magnetic field (NmA^{-1})
C: Fluid concentration
c_p: Specific heat (J/kgK)
C_f: Skin friction coefficient
D_B: Brownian diffusion of nanofluids
D_T: Thermophoretic diffusion of nanofluids
$\widetilde{E}$: Electric field intensity (NC^{-1})
$\widehat{F}_1, \widehat{F}_2$: Homotopic functions
h: Distance between the plates
J_w: Mass flux
k: Thermal conductivity $(Wm^{-1}K^{-1})$
Kr: Rotation parameter
k: The boundary parameter
M: Magnetic parameter
m: Hall parameter
n_e: Number density of electron
Nb: Brownian motion
Nt: Thermophoretic parameter
Nu: Nusselt number
O: Origen
P: Fluid pressure (Pa)
Pr: Prandtl number
Q_w: Heat flux (Wm^{-2})

q_r: Radioactive heat flux (J)
Re: Viscosity parameter
Rd: Radiation parameter
R_{ex}: Local Reynolds number
S: Cauchy stress tensor
Sc: Schmidt number
Sh: Sherwood number
t_e: Flow time (s)
T: Fluid temperature (K)
u, vw: Velocities components (ms^{-1})
u_w: Stretching velocity (ms^{-1})
x, y, z: Coordinates
X,Y: Topological space

Greek Letters:

α: Thermal diffusivity (m^2s^{-1})
η: Similarity variable
$\widehat{\kappa}$: Vertex viscosity (mPa)
κ_m: Constants where $m = 1, 2, ..$
μ: Dynamic viscosity (mPa)
v: Kinematic coefficient of viscosity
ρ_f: Base fluid density (Kgm^{-3})
ρ_b: Density of the particles (Kgm^{-3})
σ_{nf}: Electrical conductivity of nanofluid (Sm^{-1})
τ^*: Ratio of nanoparticles and heat capacity
φ: Stefan Boltzmann constant
h: Assisting parameter
Φ: Dimensional concentration profile
ω_e: Oscillating frequency of the electron (S^{-1})
Ω: Angular velocity (ms^{-1}).

Data Availability

All the relevant data is available in the manuscript.

Conflicts of Interest

All the authors declare that there is no conflict of interest regarding the publication of this paper.

References

[1] S. U. S. Choi and J. A. Estman, "Enhancing thermal conductivity of fluids with nanoparticles," in *1995 International mechanical engineering congress and exhibition*, San Francisco, CA, USA, 1995.

[2] T. Hayat, M. Khursheed, M. Farooq, and A. Alsaedi, "Squeezed flow subject to Cattaneo-Christov heat flux and rotating frame," *Journal of Molecular Liquids*, vol. 220, pp. 216–222, 2016.

[3] T. Hayat, M. Waqas, S. A. Shehzad, and A. Alsaedi, "MHD stagnation point flow of Jeffrey fluid by a radially stretching surface with viscous dissipation and Joule heating," *Journal of Hydrology and Hydromechanics*, vol. 63, no. 4, pp. 311–317, 2015.

[4] M. Sheikholeslami, M. Gorji Bandpy, and S. Soleimani, "Two phase simulation of nanofluid flow and heat transfer using heatline analysis," *International Communications in Heat and Mass Transfer*, vol. 47, pp. 73–81, 2013.

[5] M. Sheikholeslami, D. D. Ganji, and H. R. Ashorynejad, "Investigation of squeezing unsteady nanofluid flow using ADM," *Powder Technology*, vol. 239, pp. 259–265, 2013.

[6] E. A. Hamza, "The magneto hydrodynamic effects on a fluid film squeezed between two rotating surfaces," *Journal of Physics D: Applied Physics*, vol. 24, no. 4, pp. 547–554, 1991.

[7] S. Bhattacharyya and A. Pal, "Unsteady MHD squeezing flow between two parallel rotating discs," *Mechanics Research Communications*, vol. 24, no. 6, pp. 615–623, 1997.

[8] H. Alfven, "Existence of electromagnetic-hydrodynamic waves," *Nature*, vol. 150, no. 3805, pp. 405-406, 1942.

[9] M. Abd-El Aziz, "Unsteady fluid and heat flow induced by a stretching sheet with mass transfer and chemical reaction," *Chemical Engineering Communications*, vol. 197, no. 10, pp. 1261–1272, 2010.

[10] T. Hayat, M. Qasim, and Z. Abbas, "Radiation and mass transfer effects on the magnetohydrodynamic unsteady flow induced by a Stretching sheet," *Zeitschrift für Naturforschung*, vol. 65, no. 3, pp. 231–239, 2010.

[11] M. Sheikholeslami, M. Hatami, and G. Domairry, "Numerical simulation of two phase unsteady nanofluid flow and heat transfer between parallel plates in presence of time dependent magnetic field," *Journal of the Taiwan Institute of Chemical Engineers*, vol. 46, pp. 43–50, 2015.

[12] M. A. Sheremet, T. Grosan, and I. Pop, "Free convection in a square cavity filled with a porous medium saturated by nanofluid using Tiwari and Das' nanofluid model," *Transport in Porous Media*, vol. 106, no. 3, pp. 595–610, 2015.

[13] M. A. Sheremet, I. Pop, and M. M. Rahman, "Three-dimensional natural convection in a porous enclosure filled with a nanofluid using Buongiorno's mathematical model," *International Journal of Heat and Mass Transfer*, vol. 82, pp. 396–405, 2015.

[14] M. A. Sheremet, I. Pop, and N. C. Rosca, "Magnetic field effect on the unsteady natural convection in a wavy-walled cavity filled with a nanofluid: Buongiorno's mathematical model," *Journal of the Taiwan Institute of Chemical Engineers*, vol. 61, pp. 211–222, 2016.

[15] N. S. Bondareva, M. A. Sheremet, and I. Pop, "Magnetic field effect on the unsteady natural convection in a right-angle trapezoidal cavity filled with a nanofluid," *International Journal of Numerical Methods for Heat and Fluid Flow*, vol. 25, no. 8, pp. 1924–1946, 2015.

[16] M. Sheikholeslami and D. D. Ganji, "Nanofluid flow and heat transfer between parallel plates considering Brownian motion using DTM," *Computer Methods in Applied Mechanics and Engineering*, vol. 283, pp. 651–663, 2015.

[17] M. Sheikholeslami, D. D. Ganji, M. Younus Javed, and R. Ellahi, "Effect of thermal radiation on magnetohydrodynamics nanofluid flow and heat transfer by means of two phase model," *Journal of Magnetism and Magnetic Materials*, vol. 374, pp. 36–43, 2015.

[18] M. Sheikholeslami, M. M. Rashidi, and D. D. Ganji, "Ferrofluid flow and heat transfer in a semi annulus enclosure in the presence of magnetic source considering thermal radiation," *Journal of the Taiwan Institute of Chemical Engineers*, vol. 47, pp. 6–17, 2015.

[19] M. Barzegar Gerdroodbary, M. Rahimi Takami, and D. D. Ganji, "Investigation of Thermal Radiation on Traditional Jeffery–Hamel flow to stretchable convergent/divergent channels," *Case Studies in Thermal Engineering*, vol. 6, pp. 28–39, 2015.

[20] S. G. Martyushev and M. A. Sheremet, "Characteristics of Rosseland and P-1 approximations in modeling nonstationary conditions of convection-radiation heat transfer in an enclosure with a local energy source," *Journal of Engineering Thermophysics*, vol. 21, no. 2, pp. 111–118, 2012.

[21] A. Y. Bakier, "Thermal radiation effect on mixed convection from vertical surface in saturated porous media," *International Communications in Heat and Mass Transfer*, vol. 28, no. 1, pp. 119–126, 2001.

[22] R. A. Damseh, "Magnetohydrodynamics-mixed convection from radiate vertical isothermal surface embedded in a saturated porous media," *Journal of Applied Mechanics*, vol. 73, no. 1, pp. 54–59, 2006.

[23] A. Saeed, P. Kumam, T. Gul, W. Alghamdi, W. Kumam, and A. Khan, "Darcy-Forchheimer couple stress hybrid nanofluids flow with variable fluid properties," *Scientific Reports*, vol. 11, no. 1, pp. 1–13, 2021.

[24] A. Saeed, P. Kumam, S. Nasir, T. Gul, and W. Kumam, "Nonlinear convective flow of the thin film nanofluid over an inclined stretching surface," *Scientific Reports*, vol. 11, no. 1, pp. 1–15, 2021.

[25] A. Rehman, Z. Salleh, and T. Gul, "Heat transfer of thin film flow over an unsteady stretching sheet with dynamic viscosity," *Journal of Advanced Research in Fluid Mechanics and Thermal Sciences*, vol. 81, no. 2, pp. 67–81, 2021.

[26] M. Bilal, A. Saeed, T. Gul, I. Ali, W. Kumam, and P. Kumam, "Numerical approximation of microorganisms hybrid nanofluid flow induced by a wavy fluctuating spinning disc," *Coatings*, vol. 11, no. 9, p. 1032, 2021.

[27] E. K. Blum, "A modification of the Runge–Kutta fourth-order method," *Mathematics of Computation*, vol. 16, no. 78, pp. 176–187, 1962.

[28] J. C. Butcher, "The non-existence of ten stage eighth order explicit Runge–Kutta methods," *BIT*, vol. 25, no. 3, pp. 521–540, 1985.

[29] J. C. Butcher, *The Numerical Analysis of Ordinary Differential Equations*, Wiley, New York, 1987.

[30] M. H. Carpenter and C. A. Kennedy, *Fourth-Order 2N-Storage Runge–Kutta Schemes*, no. article 109112, 1994NASA TM, 1994.

[31] M. Bilal, A. Saeed, M. M. Selim, T. Gul, I. Ali, and P. Kumam, "Comparative numerical analysis of Maxwell's time-dependent thermo-diffusive flow through a stretching cylinder," *Case studies in Thermal Engineering*, vol. 27, article 101301, 2021.

[32] Z. Shah, P. Kumam, A. Dawar, and P. Thounthong, "Study of the couple stress convective micropolar fluid flow in a hall MHD generator system," *Frontiers in Physics*, vol. 7, p. 171, 2019.

[33] A. Dawar, Z. Shah, and P. Kumam, "Chemically reactive MHD micropolar nanofluid flow with velocity slips and variable heat source/sink," *Scientific Reports*, vol. 10, no. 1, pp. 1–23, 2020.

[34] A. Dawar, Z. Shah, and S. Islam, "A comparative analysis of MHD Casson and Maxwell flows past a stretching sheet with mixed convection and chmical reaction," *Waves in Random and Complex Media*, vol. 25, 2021.

[35] S. G. Bejawada, Y. D. Reddy, W. Jamshed, K. S. Nisar, A. N. Alharbi, and R. Chouikh, "Radiation effect on MHD Casson fluid flow over an inclined non-linear surface with chemical reaction in a Forchheimer porous medium," *Alexandria Engineering Journal*, vol. 61, no. 10, pp. 8207–8220, 2022.

[36] T. C. Sun, I. Uddin, M. A. Zahoor Raja et al., "Numerical investigation of thin-film flow over a rotating disk subject to the heat source and nonlinear radiation: Lobatto IIIA approach," *Waves in Random and Complex Media*, vol. 10, pp. 1–15, 2022.

[37] W. Jamshed, R. Safdar, A. Brahmia, A. K. Alanazi, H. M. Abo-Dief, and M. R. Eid, "Numerical simulations of environmental energy features in solar pump application by using hybrid nanofluid flow: Prandtl-Eyring case," *Energy & Environment*, vol. 15, pp. 1–44, 2022.

[38] F. Shahzad, W. Jamshed, A. Koulali et al., "Computational examination of Jeffrey nanofluid through a stretchable surface employing Tiwari and Das model," *Open Physics*, vol. 19, no. 1, pp. 897–911, 2021.

[39] W. Jamshed, A. K. Alanazi, S. S. P. Mohamed Isa et al., "Thermal efficiency enhancement of solar aircraft by utilizing unsteady hybrid nanofluid: a single-phase optimized entropy analysis," *Sustainable Energy Technologies and Assessments*, vol. 52, article 101898, 2021.

[40] S. G. Bejawada, W. Jamshed, R. Safdar et al., "Chemical reactive and viscous dissipative flow of magneto nanofluid via natural convection by employing Galerkin finite element technique," *Coatings*, vol. 12, p. 151, 2022.

[41] S. E. Alhazmi, F. Wang, U. Nazir et al., "Utilization of modified fluxes on thermal and mass transportation in Williamson material," *Advances in Mechanical Engineering*, vol. 14, no. 1, 2022.

[42] M. Ouni, L. M. Ladhar, M. Omri, W. Jamshed, and M. R. Eid, "Solar water-pump thermal analysis utilizing copper–gold/engine oil hybrid nanofluid flowing in parabolic trough solar collector: thermal case study," *Case Studies in Thermal Engineering*, vol. 30, p. 101756, 2022.

[43] N. Herisanu and V. Marinca, "An efficient analytical approach to investigate the dynamics of a misaligned multirotor system," *Mathematics*, vol. 8, no. 7, p. 1083, 2020.

[44] N. Herisanu, V. Marinca, G. Madescu, and F. Dragan, "Dynamic response of a permanent magnet synchronous generator to a wind gust," *Energies*, vol. 12, no. 5, p. 915, 2019.